Question 1

a.

The eddy-uv case is a special case of solutions to the 2D incompressible NS equations (the NS momentum equation is reproduced below)

$$\rho\left(\frac{\partial u_i}{\partial t} + u_j\frac{\partial u_i}{\partial x_j}\right) = -\frac{\partial p}{\partial x_i} + \mu\frac{\partial^2 u_i}{\partial x_j\,\partial x_j} + f_i$$

The solution is an artificial solution on a double periodic domain (ie, period in x and in y). The initial conditions and solution are composed of a series of eigenfunctions making up a series. The nature of the solution allows for a closed-form solution across time, which is a rarity (closed-form transient solutions to NS are not common). Comparing the SEM solution to the analytical solution allows verification of the code.

b.

Both solutions, at Re=20 and Re=100, were run for 2000 timesteps at dt=1e-4s, for a total of 0.2s of simulated time. Both solutions were run with 15th-order elements.

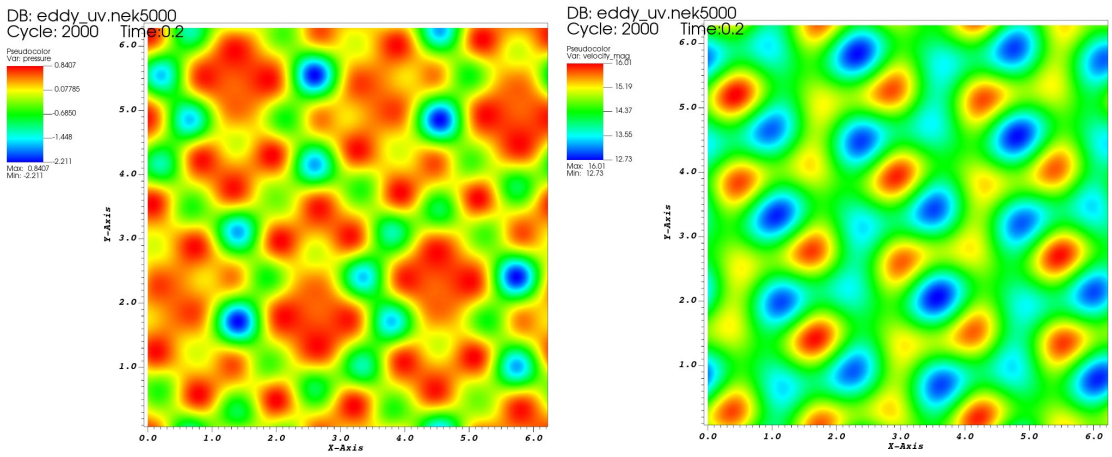

Figure 1: Pressure and velocity snapshot at Re=20

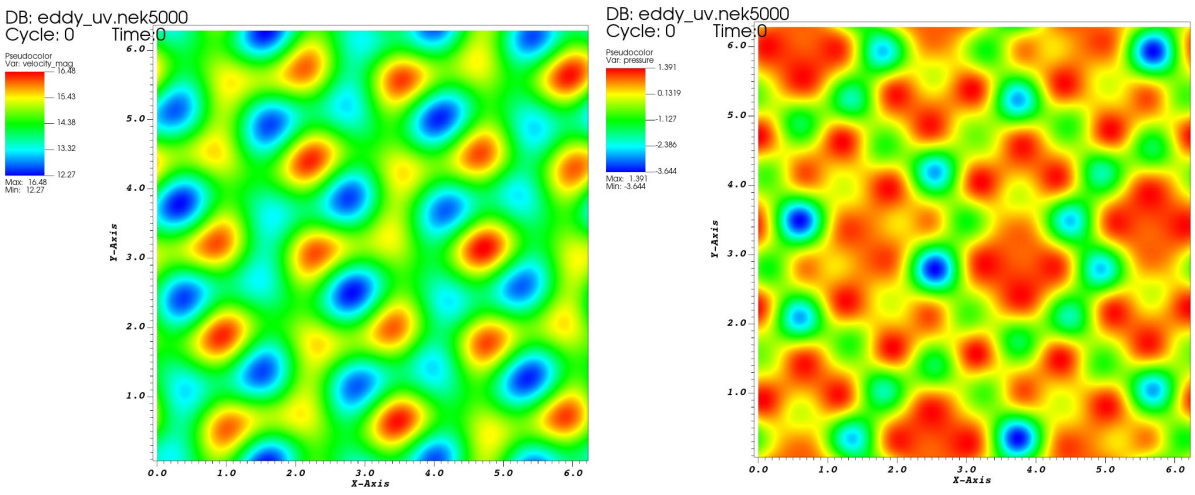

Figure 2: Pressure and velocity snapshot at Re=100

The only visible difference between the two solutions is the magnitude of the solution. Plotting a glyph of the velocity shows the eddies:

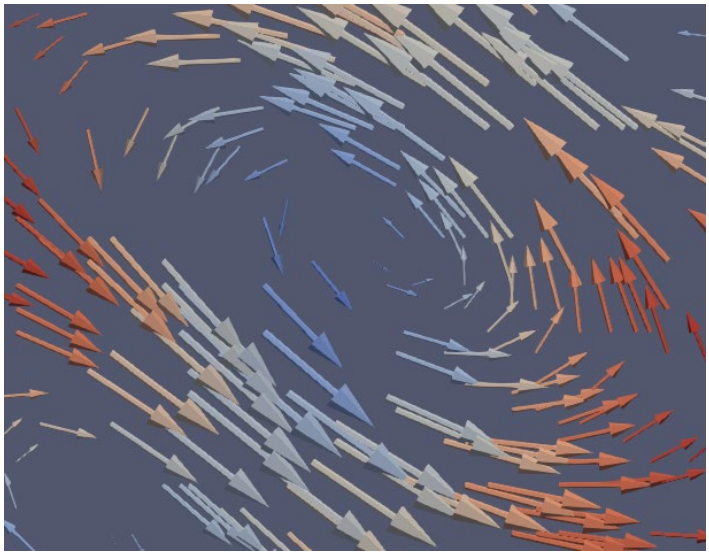

Figure 3: Velocity glyph

The velocity and pressure fields advect up and to the right, and they are maintained in a coherent manner. The difference is marginal between the two cases at Re=20 and Re=100, but at low Reynolds numbers the vortices would be expected to diffuse more. As they advect to the top and right, they reappear at the bottom left, in accordance with the doubly-periodic boundary condition.

C.

The error with the initial parameters and Re=100 is quite large. It is plotted below in Fig. 4.

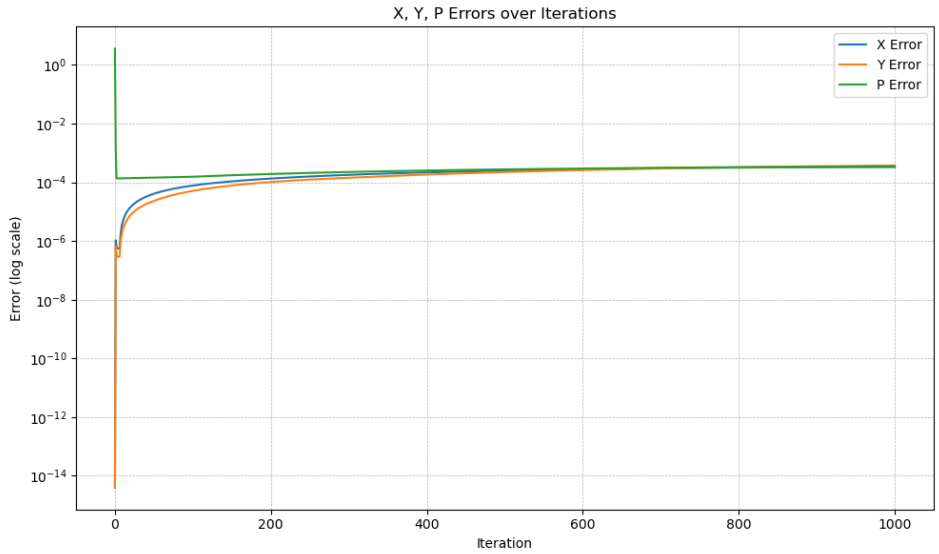

Figure 4: Error with initial case setup

Changing the polynomial order to 15 and the timestep to 1e-5 (from 1e-4) results in much lower error against the analytical solution. The error is on the order of 1e-12 for the x- and y- error, which is not far off double machine precision (1e-16).

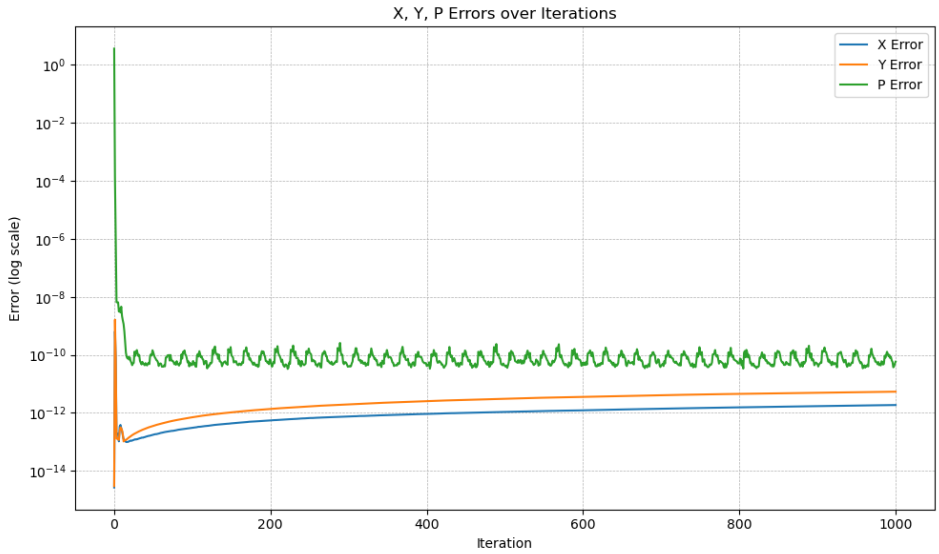

Figure 5: Error with modified case setup

d.

The error in the simulation results from truncation errors and round-off errors. There is a finite threshold for how low the error can be driven. Truncation error is decreased by using higher-order polynomials or more elements (which are both equivalent to adding degrees of freedom). Roundoff error is a necessary evil with floating-point computing. It could be driven by using quad arithmetic instead of double arithmetic but the cost is most likely not worth it.

Question 2

a.

This is the typical external flow past a cylinder problem. Once again, the PDE in question is the incompressible NS:

$$\rho\left(\frac{\partial u_i}{\partial t} + u_j\frac{\partial u_i}{\partial x_j}\right) = -\frac{\partial p}{\partial x_i} + \mu\frac{\partial^2 u_i}{\partial x_j\,\partial x_j} + f_i$$

A cylinder is simulated inside a uniform left-to-right flow. The boundary condition is no-slip and no-penetration along the cylinder surface. The top and bottom boundary conditions are flow-through, the left boundary condition is an inflow, and the right boundary condition is an outflow.

b.

Below, the velocity magnitude at the final iteration is plotted for various Reynolds numbers.

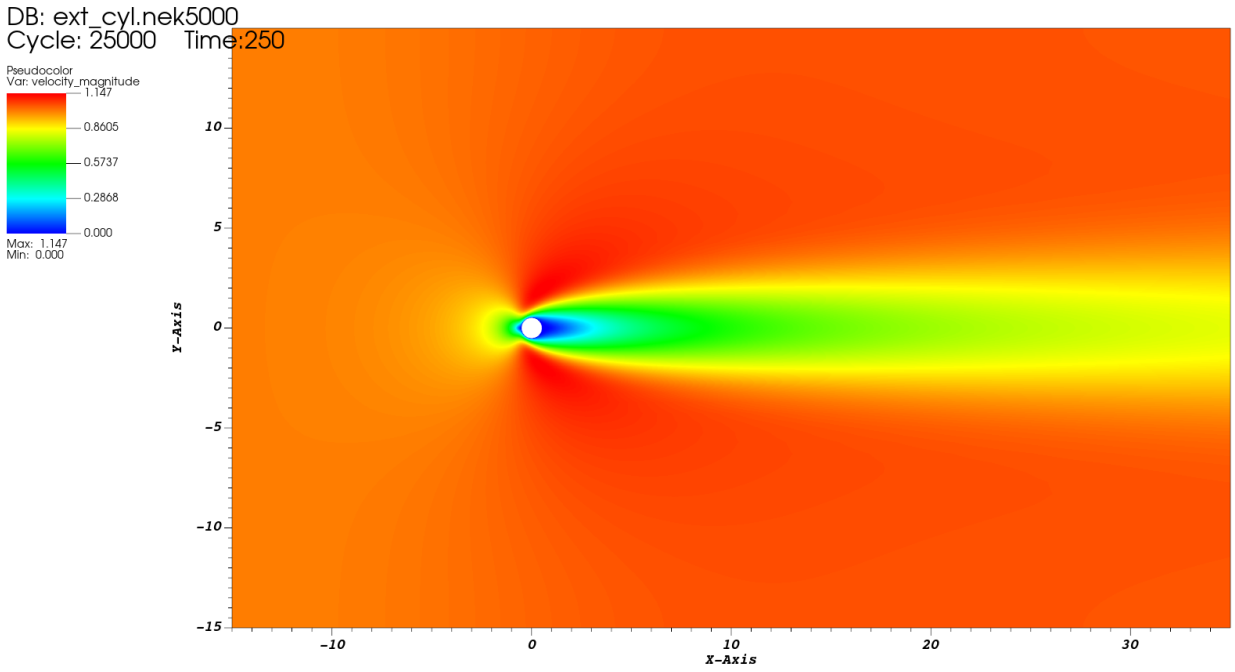

Figure 6: External cylinder flow at Re=10. The wake is very wide and no oscillations or vortex-shedding is observed.

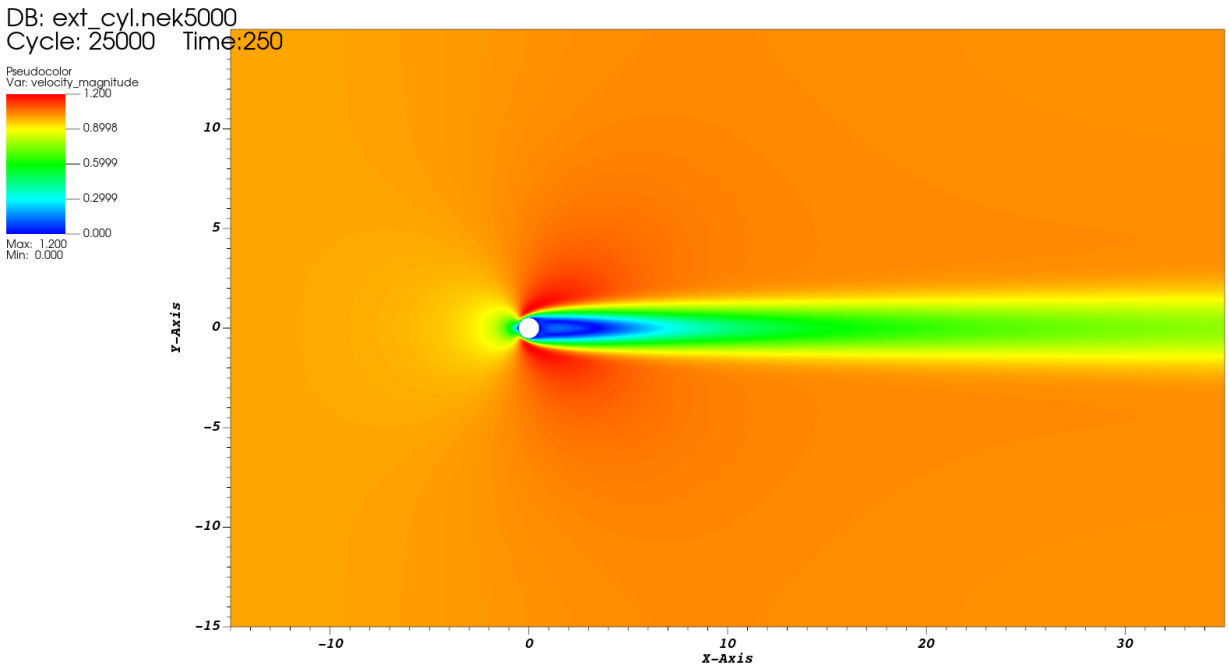

Figure 7: External cylinder flow at Re=50. The wake is stronger, longer, and thinner, but still no oscillations or vortex-shedding is observed.

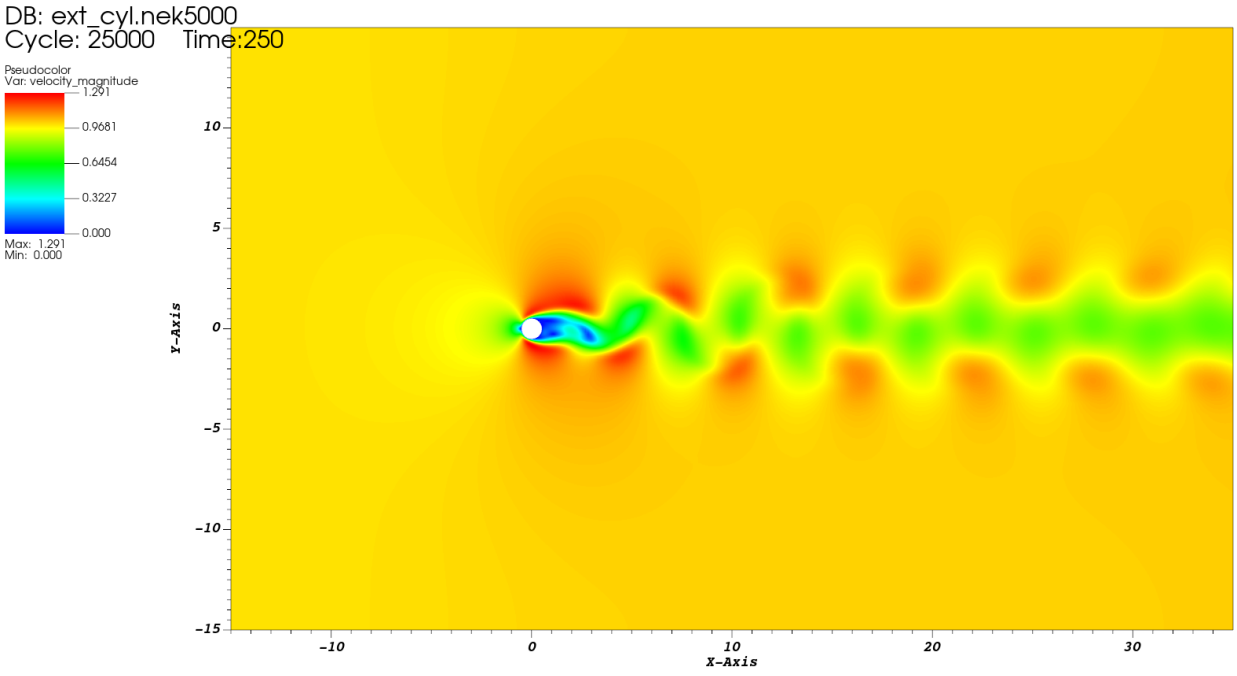

Figure 8: External cylinder flow at Re=75. Vortex shedding has begun.

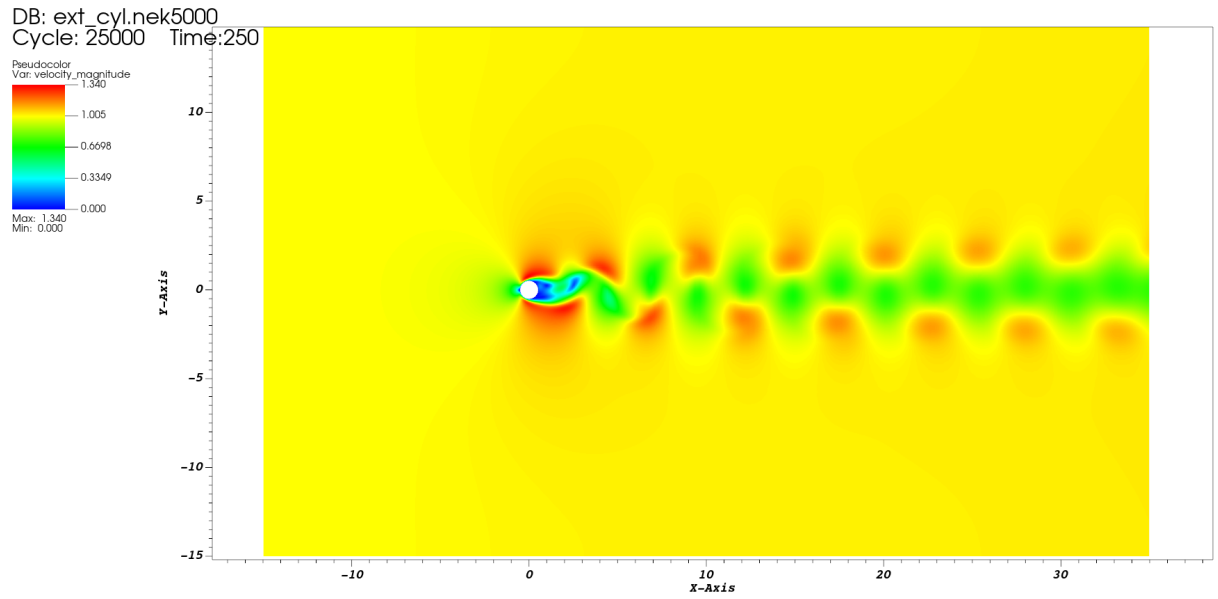

Figure 6: External cylinder flow at Re=100. The shed vortices appear smaller and at higher frequency than at Re=75

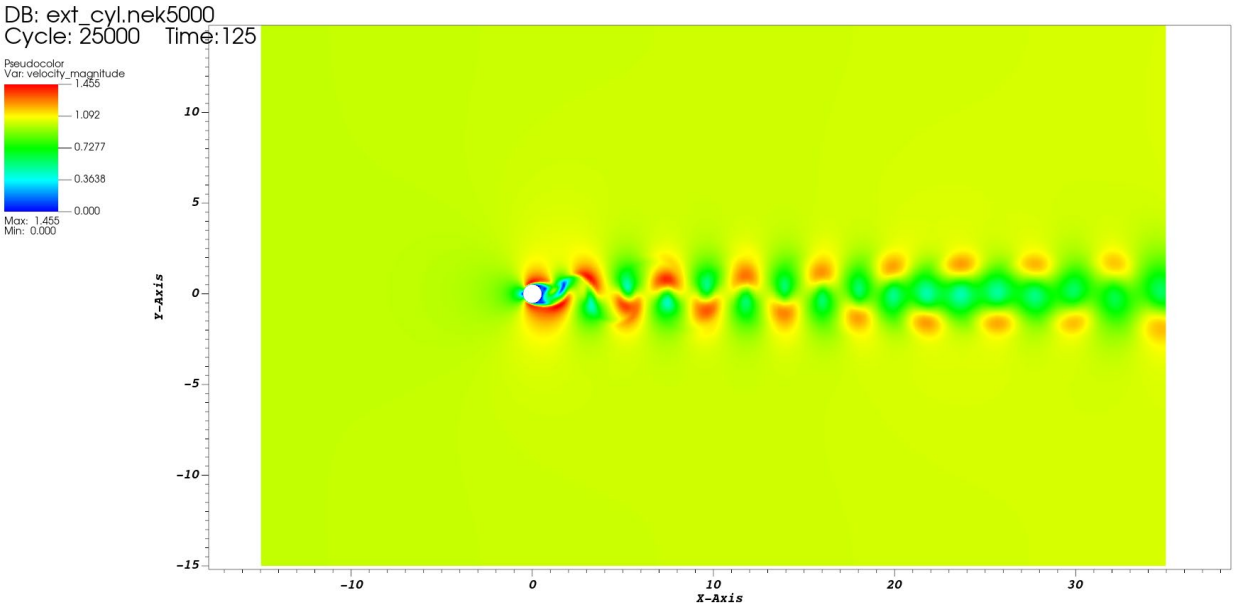

Figure 8: External cylinder flow at Re=250. The shed vortices are much smaller and higher frequency.

Based on this range of cases, I expect that vortex shedding in this flow begins at a Reynolds number between 50-75. This aligns with the literature, which generally highlights Re~50-60 as the point where vortex shedding begins around a bluff body in a 2D flow.

C.

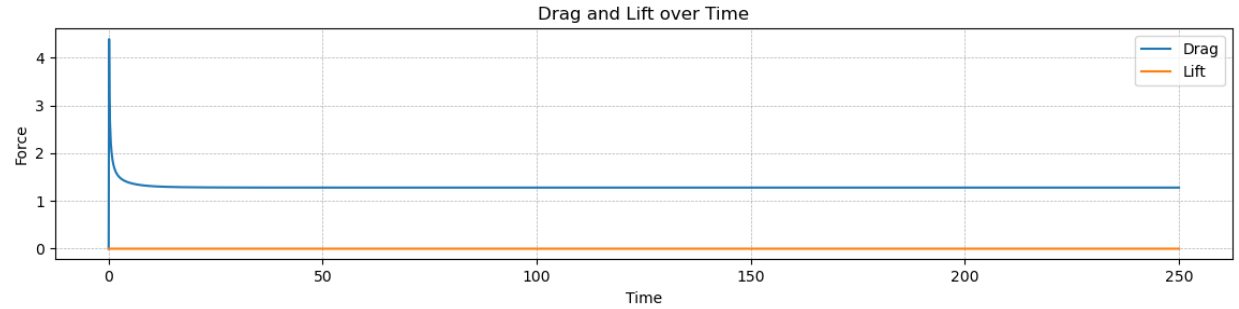

Figure 9: Drag and lift over time at Re=10

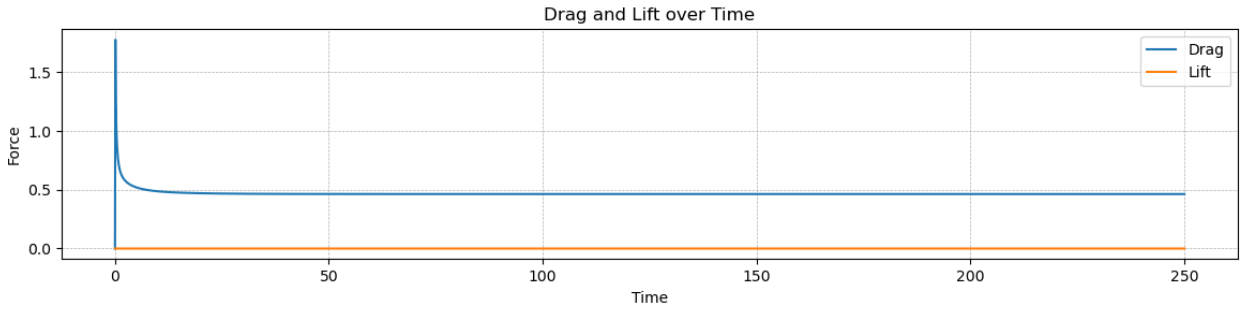

Figure 10: Drag and lift over time at Re=50

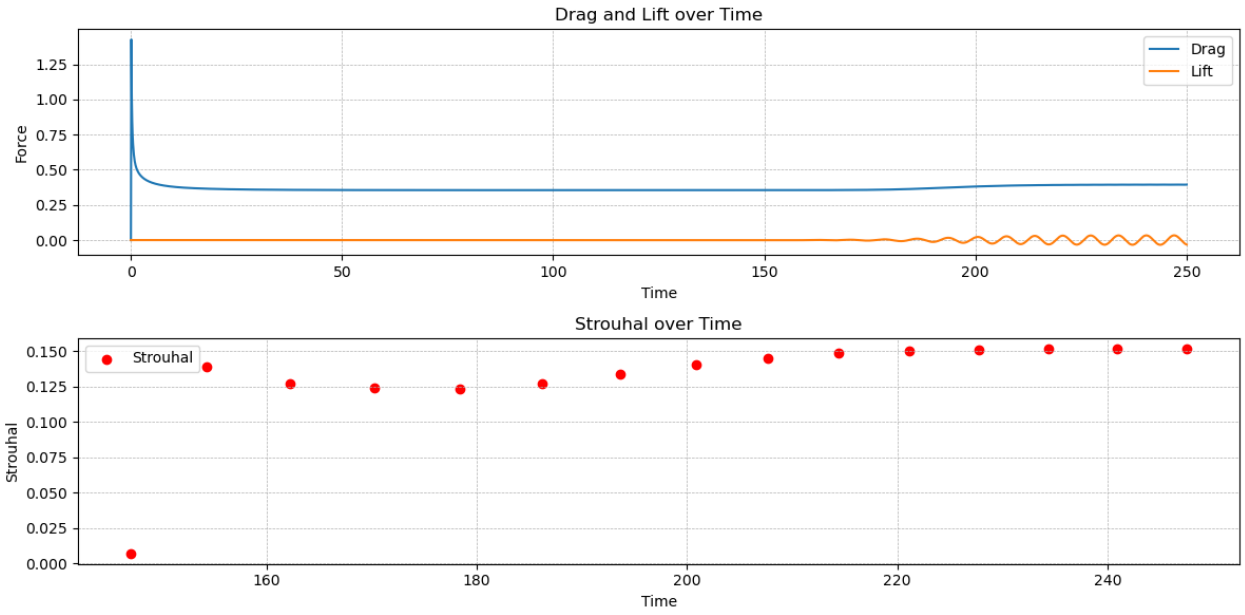

Figure 11: Drag and lift over time at Re=75

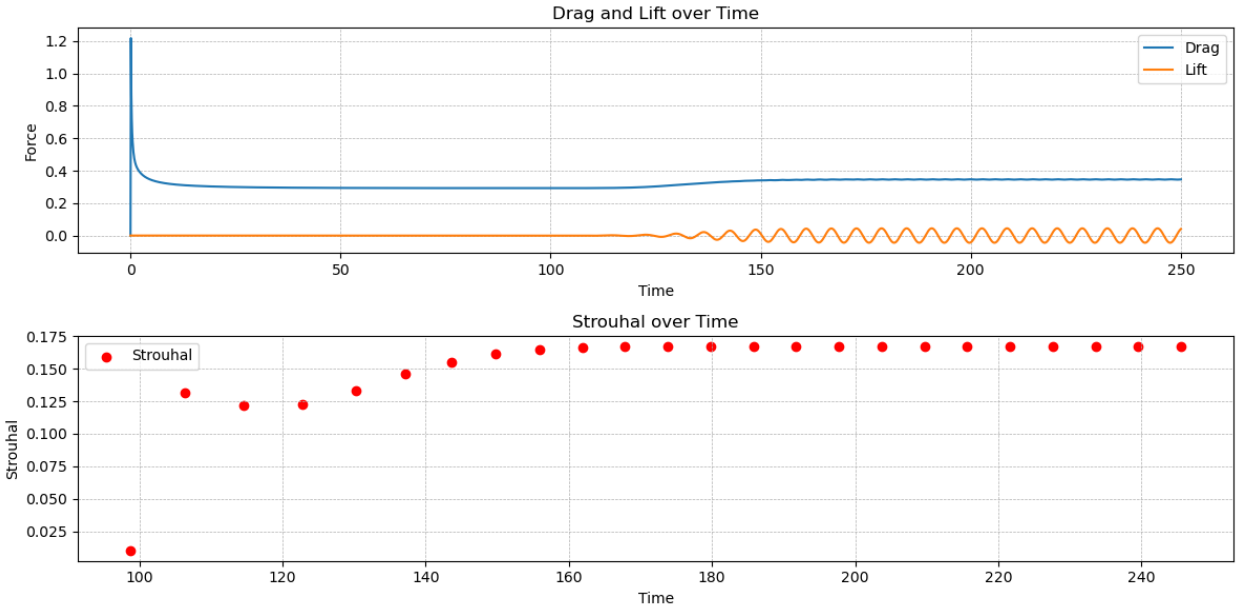

Figure 12: Drag and lift over time at Re=100

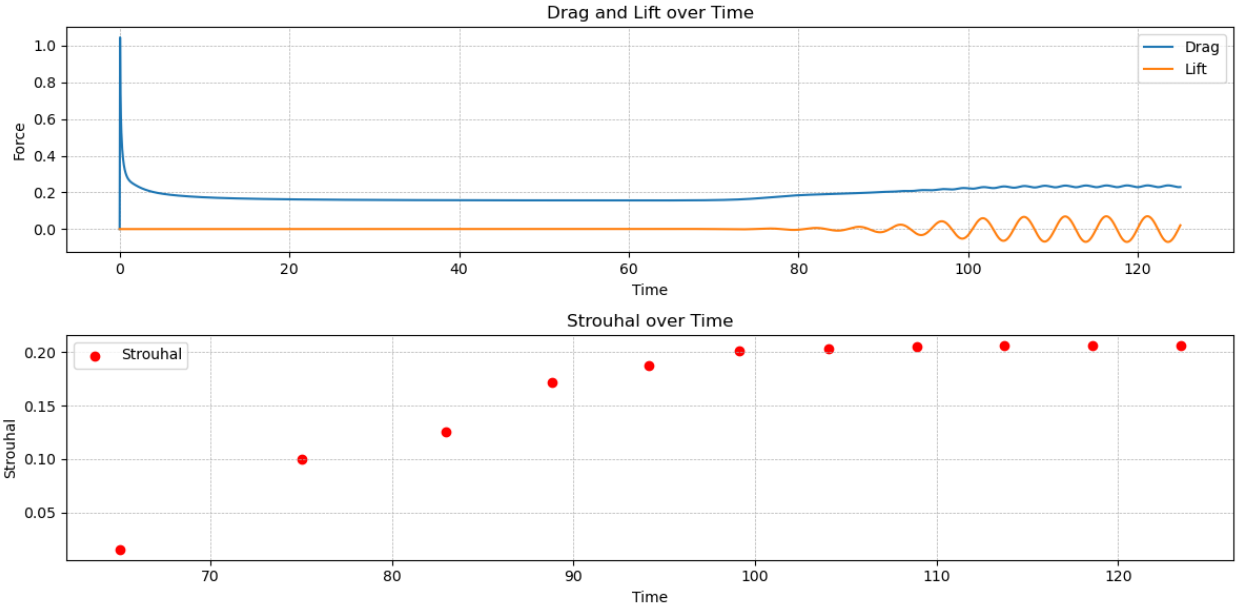

Figure 13: Drag and lift over time at Re=10

The drag and lift for all the cases, as well as the Strouhal number for cases Re>75 where vortex shedding is observed, is plotted above. The behavior aligns with the behaviors observed in full plots of the solution for part b.

The steady, time averaged values for lift, drag, and Strouhal number are plotted below.

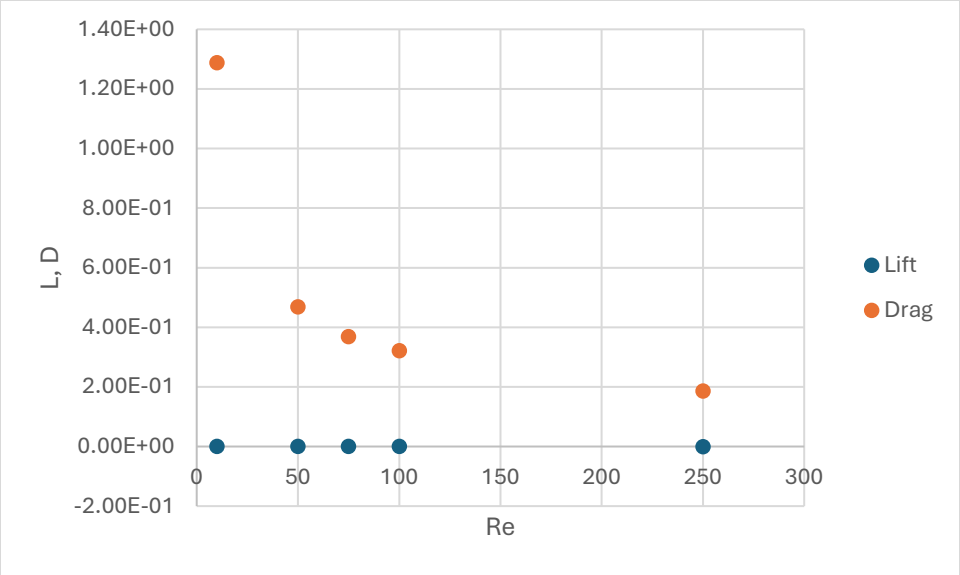

Figure 14: Steady values for lift and drag

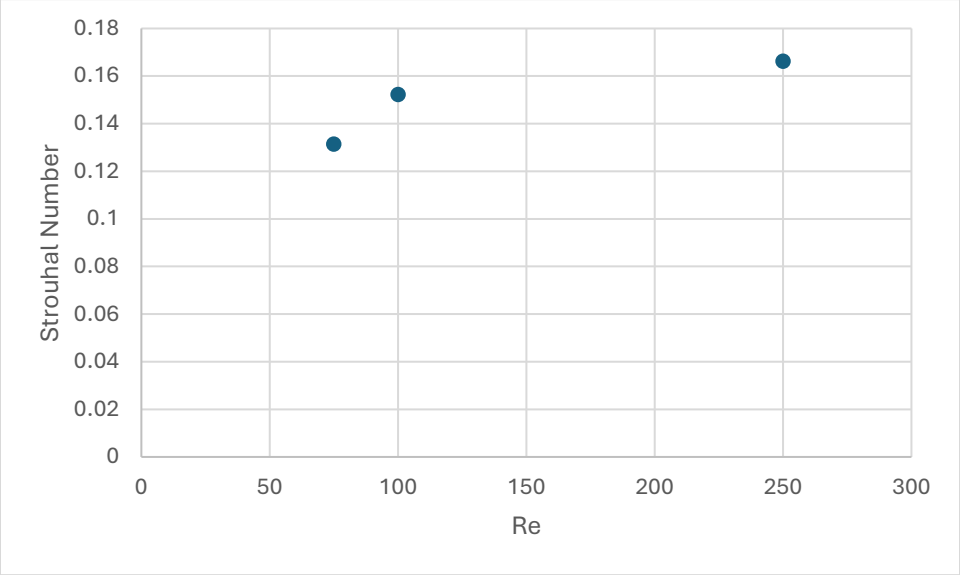

Figure 15: Steady value for Strouhal number

As expected, the lift on a non-rotating cylinder is 0. Drag decreases with Reynolds number, which is generally observed for spheres and cylinders. The Strouhal number increases with Re, although firm conclusions about the Strouhal number are difficult to make with only 3 data points.

d.

To prove grid convergence, the Re=250 case was run again with 12th-order GLL elements. This necessitated a decrease in the timestep to 2.5e-4. Grid convergence is evaluated by plotting the lift and drag against the lift and drag for the 6th-order element case.

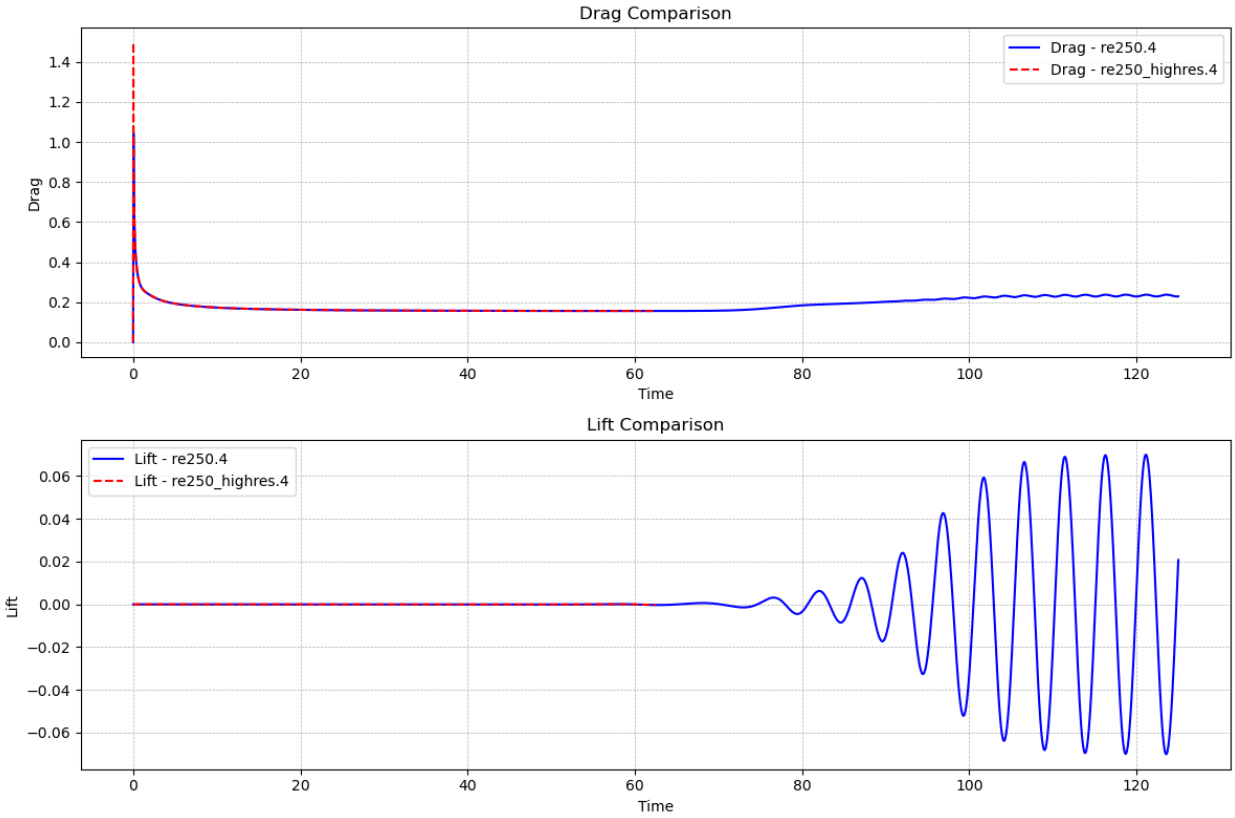

Agreement is observed, indicating that grid convergence has been reached. Due to the smaller timestep, only half of the time was simulated in the high-resolution case (I didn't have time to run the high-res case on my machine before turning this in). So, the indication of grid convergence is not definitive.